Crystallographic dependence of visible-light photoactivity in epitaxial $TiO_{2-x}N_x$ anatase and rutile

T. Ohsawa,[1] I. Lyubinetsky,[2] Y. Du,[2] M. A. Henderson,[1]
V. Shutthanandan,[2] and S. A. Chambers[1]
[1]*Materials and Chemical Sciences Division, Fundamental and Computational Sciences Directorate, Pacific Northwest National Laboratory, Richland, Washington 99352, USA*
[2]*Environmental Molecular Sciences Laboratory, Pacific Northwest National Laboratory, Richland, Washington 99352, USA*
(Received 2 December 2008; published 3 February 2009)

Nitrogen-doped TiO_2 materials have been shown to exhibit visible-light photoactivity, but the operative mechanism(s) are not well understood. Here we use structurally and compositionally well-defined epitaxial films of $TiO_{2-x}N_x$ anatase (001) and rutile (110) ($x \leq \sim 0.02$) to show a qualitative difference between the visible-light activities for the two polymorphs. Holes generated by visible light at N sites in anatase (001) readily diffuse to the surface and oxidize adsorbed trimethyl acetate while the same in rutile (110) remain trapped in the bulk. In light of the low doping densities that can be achieved in phase-pure material, conventional wisdom suggests that holes should be trapped at N sites in both polymorphs. Although the detailed mechanism is not yet understood, these results suggest that the hole hopping probability is much higher along the [001] direction in N-doped anatase than along the [110] direction in N-doped rutile.

DOI: 10.1103/PhysRevB.79.085401 PACS number(s): 73.61.Le, 72.20.−i

I. INTRODUCTION

Much effort has been devoted to heterogeneous photocatalysis using oxide semiconductors. Titanium dioxide, TiO_2, has been widely used since its utility for photoelectrolysis of water was first reported.[1] TiO_2 has also attracted much attention for use in dye-sensitized solar cells[2,3] and the photodecomposition of organic pollutants.[4,5] However, with a 3 eV bandgap, TiO_2 absorbs relatively little of the solar spectrum. Asahi *et al.*[6] first suggested that nitrogen doping reduces the bandgap. There have since been a plethora of publications describing enhanced visible-light photochemical activity in N-doped TiO_2 nanoparticles. While intriguing, these studies lack the in-depth materials understanding required to establish defensible cause-and-effect relationships between composition/structure and electronic structure/photochemical properties. Such determinations are difficult in light of the heterogeneous, multiple-orientation, and defective nature of nanoparticle assemblies. Electronic structure calculations have also provided conflicting information.[7–11] A common feature is that at low N doping levels, the N-derived states are localized about N and fall at midgap or close to the valence-band maximum in the host oxide. Some calculations predict an increase in bandgap for N-doped rutile,[7] at odds with experimental results,[12,13] but most predict a decrease in the optical absorption threshold. The absence of band formation at typical doping levels suggests that holes created by light absorption should become trapped at N sites, precluding surface photoactivity. The goal of the present work is to address this issue by undertaking fundamental photocatalytic studies using N-doped epitaxial films of both anatase (001) and rutile (110). We have used the hole-mediated photodecomposition of trimethyl acetate (TMA) as a probe of photochemical activity. No such investigations in which the photochemical activity of structurally and compositionally well-defined epitaxial films of N-doped anatase and rutile is directly compared have been reported to the best of our knowledge.

II. EXPERIMENTAL DETAILS

All films were grown by plasma-assisted molecular-beam epitaxy (PAMBE) in a custom chamber described elsewhere.[14] Epitaxial films of $TiO_{2-x}N_x(001)$ ($x \leq \sim 0.02$) anatase were grown by PAMBE on undoped or Nb-doped (0.02 at. %) $SrTiO_3(001)$ (STO) and undoped $LaAlO_3(001)$ (LAO). Similarly, $TiO_{2-x}N_x(110)$ ($x \leq \sim 0.02$) rutile epifilms were grown on rutile $TiO_2(110)$. The growth and physical properties of N-doped anatase on LAO(001) and N-doped rutile on $TiO_2(110)$ have been described in detail elsewhere.[12,13,15] In Sec. III A, we describe the growth details for N-doped anatase on STO(001). The maximum N concentration that can be substitutionally incorporated in phase-pure anatase and rutile is ~1 at. % ($TiO_{2-x}N_x$, where $x = \sim 0.02$). We have found that if growth conditions are modified such that the *apparent* N concentration exceeds this value, secondary phase formation has in fact occurred and the resulting properties cannot be ascribed to phase-pure N-doped TiO_2. N doping in phase-pure anatase and rutile reduces the optical absorption threshold into the visible for both polymorphs.

The PAMBE chamber is connected to an x-ray photoelectron spectrometer (XPS) chamber and a photodesorption chamber, allowing sample transfer under ultrahigh vacuum conditions. The former is equipped with a Gamma Data/Scienta SES 200 analyzer and a monochromatic Al $K\alpha$ x-ray source. The latter includes a molecular dosing apparatus for trimethyl acetic acid (TMAA), the precursor of TMA, an Hg arc lamp, and a quadrupole mass spectrometer. The STO substrates were etched in buffered HF and annealed in flowing O_2 at 1 atm at 950 °C for 8 h. The etch dissolved SrO terraces and the oxygen anneal resulted in mass transport of the discontinuous TiO_2 microterraces, resulting in an atomically flat, TiO_2 terminated surface with a minimum step height of 4 Å.[16] This treatment left some residual fluorine on the surface which could not be removed by annealing. The

measured F 1*s* binding energy was ~684.0 eV, which is close to that exhibited by SrF_2, −684.6 eV.[17] Based on this binding energy and the high degree of thermal stability, we conclude that F substitutes for O in the lattice. Under this assumption and using atomic photoemission cross sections,[18] the F mole fraction within the anion sublattice is estimated to be ~0.05 within the probe depth of XPS at normal emission (~45 Å).

Following sonication in acetone and isopropanol along with UV/ozone cleaning on the bench, the substrates were loaded into the PAMBE chamber and exposed to activated oxygen from the electron cyclotron resonance (ECR) plasma at a chamber pressure of 2×10^{-5} Torr for 1 h. This treatment left the surfaces clean with the exception of F, as judged by XPS. Activated O and N were supplied from an ECR plasma source. O_2 and N_2 were streamed into the plasma cup at approximately equal flow rates. The chamber pressure during growth was $\sim2\times10^{-5}$ Torr. The Ti beam was supplied from a high-temperature effusion cell. All films were grown at a substrate temperature of 575 ± 50 °C, as judged by a two-color infrared pyrometer. All growths were carried out under oxygen-rich conditions, with an O/O_2 to Ti flux ratio of $\geq\sim100$. The growth rate was ~0.5 ML TiO_2 anatase per minute.

Scanning tunneling microscopy (STM) experiments were carried out *ex situ* in a variable-temperature STM system (Omicron) with an electrochemically etched W tip. This chamber is also equipped with a molecular dosing apparatus for TMAA and an Hg arc lamp. Anatase (001) epifilms were transferred rapidly through air from the OPAMBE chamber to the STM system and were cleaned by light Ar ion sputtering and annealing at ~600 °C in UHV, resulting in a (1×4) reconstructed surface with a well-defined terrace-step structure.

The photochemical activity of the resulting surfaces was probed using hole-mediated photodecomposition of TMA which results from acid dissociation of TMAA on the surface. Characterization of the process was carried out using high-energy-resolution XPS, photodesorption spectrometry (PS), and STM. The light source was an Hg arc lamp with cutoff filters when elimination of the UV lines was desired. TMA photodecomposition is a sensitive probe of surface photochemical activity. TMAA undergoes acid dissociation on the anatase (001) and rutile (110) surfaces, leading to TMA that is bound to undercoordinated surface Ti atoms and acid protons that bind to surface O atoms.[19] TMA photodecomposition is initiated by interaction with a photogenerated hole followed by destabilization and decomposition to CO_2 and an organic fragment.[20] TMA surface coverage change was monitored as a function of light exposure by either directly counting the number of adsorbed anions remaining after a given light dose using STM or dynamically by PS, using mass 44 (CO_2) as a probe of the instantaneous photodesorption rate. Absolute TMA coverages were determined by XPS.

III. RESULTS AND DISCUSSION

A. As-grown TiO_2 and $TiO_{2-x}N_x$ anatase/*n*-$SrTiO_3$(001)

Figure 1 shows typical RHEED patterns for an

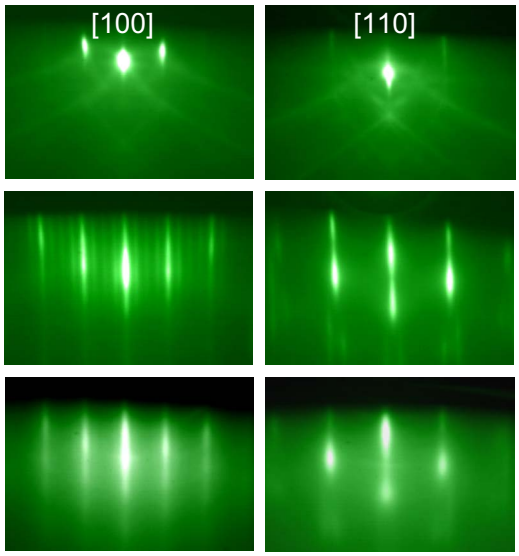

FIG. 1. (Color online) Reflection high-energy electron diffraction (RHEED) patterns for *n*-$SrTiO_3$(001) (top) and epitaxial $TiO_{2-x}N_x$ anatase with $x=0$ (middle) and $x=0.02$ (bottom) along the [100] and [110] zone axes.

n-STO(001) substrate (top row), as well as 30-nm-thick films of undoped anatase TiO_2 (middle row) and anatase $TiO_{1.98}N_{0.02}$ (bottom row) in the [100] and [110] zone axes. The sharp spot patterns for the substrate and more streaky film patterns are consistent with the atomically flat surfaces and well-defined terrace-step structure seen in the STM images (discussed below). The (1×4) reconstruction streaks are clearly seen in the [100] zone axis pattern for the undoped film but are somewhat blurred in the doped film pattern.

We show in Fig. 2 high-resolution XRD scans for a typical 30 nm film of anatase $TiO_{1.98}N_{0.02}$ grown on a 30 nm film of pure anatase TiO_2 on *n* STO(001). The θ-2θ scan [Fig. 2(a)] reveals that the majority phase is (001)-oriented anatase. The anatase (004) peak is asymmetric to higher Bragg angle, as seen in the inset. The Bragg angle scale was calibrated using the STO (002) reflection as an internal standard. On the basis of this calibration, the *c* lattice parameter determined from the Bragg angle at the anatase (004) peak maximum is 9.557 Å, which exceeds that of bulk anatase by 0.44%. The Bragg angle for bulk anatase is marked with a dashed line in the inset. The in-plane lattice mismatch between anatase and STO is −3.1%, resulting in the anatase film being in tension when coherently or semicoherently strained. Therefore, any residual strain associated with the lattice mismatch would tend to reduce *c* relative to the bulk value. The fact that *c* for the N-doped anatase film *exceeds* the bulk value is most likely due to lattice expansion associated with N substitution for O. Substitutional N is present in the lattice as N^{3-}, as explained below. The ionic radius of N^{3-} is 1.46 Å, whereas that for O^{2-} is 1.36 Å,[21] and expansions in the Ti-N bond lengths relative to those for Ti–O have been predicted for N-doped anatase and rutile.[7] Therefore, we expect a measurable lattice expansion as a result of N substitution for O. Indeed, *a* and *c* were seen to expand by 0.5% and 0.8%, respectively, as a result of N substitution for

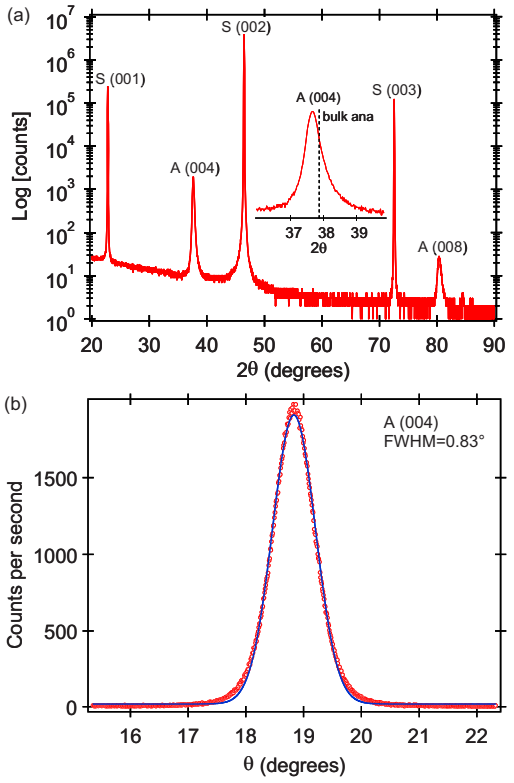

FIG. 2. (Color online) (a) High-resolution x-ray diffraction (XRD) $\theta-2\theta$ and (b) rocking curve measurements for 30 nm anatase $TiO_{1.98}N_{0.02}/30$ nm TiO_2/n-$SrTiO_3(001)$. The solid blue curve in (b) is a fit to the data to determine the full width at half maximum (FWHW).

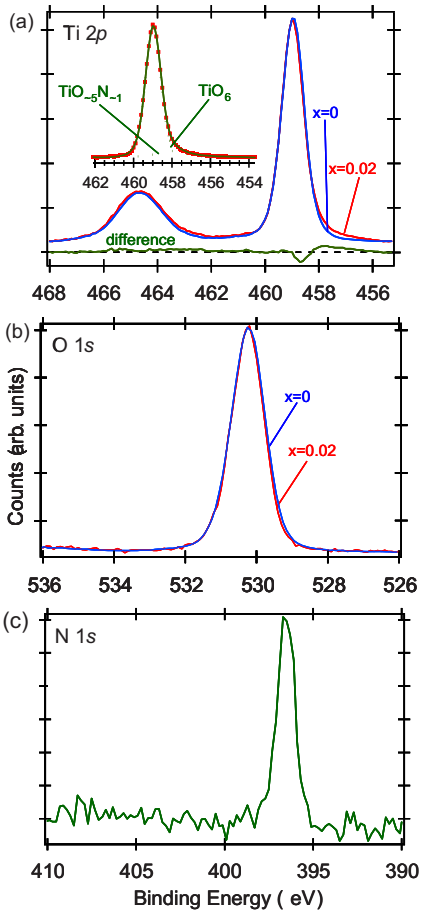

FIG. 3. (Color online) High-energy-resolution core-level spectra for epitaxial $TiO_{2-x}N_x$ anatase on n-$SrTiO_3(001)$ for $x=0$ and $x=0.02$: (a) Ti $2p$, with curve fitting of chemically inequivalent Ti $2p_{3/2}$ peaks in the inset; (b) O $1s$; (c) N $1s$.

O in homoepitaxial N-doped rutile (110).[12,13] At the same time, the presence of diffraction intensity at the Bragg angle expected for bulk anatase associated with the peak asymmetry is most likely due to the presence of undoped anatase, which was grown before growing the doped film for this particular specimen.

Figure 2(b) shows the rocking curve measurement for the anatase (004) reflection. The large width suggests a distribution of crystal orientations as expected if the film has high mosaic spread. High mosaic spread may occur given the high lattice mismatch.

Figure 3 shows high-resolution XPS spectra obtained immediately after growth for typical anatase TiO_2 and $TiO_{1.98}N_{0.02}$ epitaxial films. There is no evidence of reduced Ti(III) in the Ti $2p$ spectrum [Fig. 3(a)] which might be expected if N substitution for O facilitates O vacancy formation, as some have suggested.[7,8,10,22–26] Ti(III) typically exhibits a Ti $2p_{3/2}$ binding energy ~2 eV lower than that of fully oxidized Ti(IV). There is a weak shoulder shifted ~1.0 eV to lower binding energy relative to the normal Ti $2p$ lattice peak in the doped film which is consistently present in N-doped TiO_2 for both rutile and anatase polymorphs.[12,13,15] Upon curve fitting [inset of Fig. 3(a)], it was found that the area of this feature grows in proportion to the N dopant concentration. We thus assign this peak to Ti bound on average to ~5 O ligands and ~1 N ligand. The binding energy is lower by virtue of the lower electronegativity of N compared to O. Assuming a random N distribution, the area of this peak divided by the entire Ti $2p_{3/2}$ peak area can be compared to the fraction of Ti atoms bound to one N, as computed using the binomial theorem, in order to estimate x. Doing so yields values in qualitative agreement with the x value determined by comparing the N $1s$ and O $1s$ peak areas, corrected for photoemission cross section.[18] The presence of this peak constitutes indirect evidence that N substitutes for O in the lattice. More direct evidence for N substitution for O comes from nuclear reaction analysis (NRA) using the $^{14}N(d,\alpha)^{12}C$ and $^{16}O(d,p)^{17}O$ nuclear reactions excited by 0.95 MeV deuterons. The N reaction yield minimizes along the surface normal, as does the O reaction yield and the Ti backscattering yield using 2.0 MeV He ions at a scattering angle of 150°. The surface normal is a channeling direction for both Ti and O in anatase (001). The minimum yields for all three elements are ~50%, as expected if a high degree of mosaic spread is present, as suggested by XRD.

The O $1s$ spectra are virtually identical for undoped and doped films, as seen in Fig. 3(b). There is no change in line shape. Thus, N incorporation does not perturb the O sublattice in a measurable way other than the substitution event itself and the associated slight extent of lattice expansion

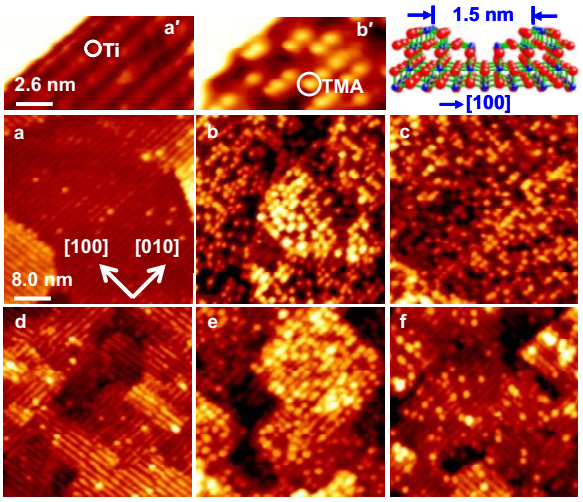

FIG. 4. (Color online) STM images of epitaxial $TiO_{2-x}N_x$ anatase/*n*-$SrTiO_3$(001) with and without saturation doses of TMA and before and after visible-light irradiation: (a, a′) $x=0$, clean; (b, b′) $x=0$, TMA, no irradiation, where a′ and b′ are higher magnification images of a and b; (c) $x=0$, TMA, after visible-light exposure (5.64×10^{20} photons/cm^2); (d) $x=0.02$, clean; (e) $x=0.02$, TMA, no irradiation; (f) $x=0.02$, TMA, after visible-light exposure (5.64×10^{20} photons/cm^2). The individual TMA anions appear as bright lobes, separated by ~1.2 and ~1.5 nm along [010] and [100], respectively. Also shown is a structural diagram for the clean (1×4) reconstructed surface.

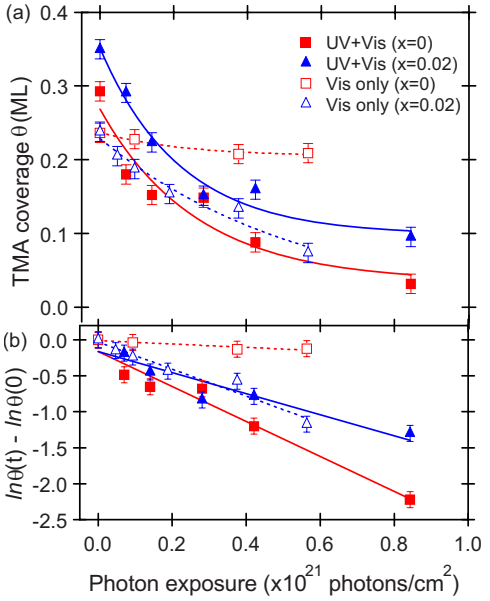

FIG. 5. (Color online) (a) STM-derived TMA coverages vs photon dose for epitaxial $TiO_{2-x}N_x$ anatase/*n*-$SrTiO_3$(001) at $x=0$ and 0.02. The lines are fits to simple exponentials that yield the photodissociation/desorption composite rate constants; (b) natural logarithm of TMA coverage vs photon dose. The photon fluxes for UV-plus-visible and visible light only were 1.2×10^{17} cm^{-2}-sec^{-1} and 2.6×10^{16} cm^{-2}-sec^{-1}, respectively.

discussed above. The N 1*s* spectrum consists of a single peak at 396.6 eV, which is characteristic of N^{3-}. In the absence of other effects, we expect substitutional N to be N^{2-}, as it is in TiN. The N 1*s* binding energy in TiN is 397.7 eV, and the Ti 2*p* spectrum is characteristic of Ti(II).[27] Thus, N is clearly present as N^{2-} in TiN. Upon substitution for O as N^{2-}, the reduction in N to the −3 state may occur because the 2*p* holes on the N^{2-} species are compensated by itinerant electrons from interstitial Ti(III), analogous to what occurs during N-doped rutile homoepitaxy on TiO_2(110) rutile.[12,13,15]

B. TMA on N-doped anatase (001) and rutile (110) epitaxial films

We show in Fig. 4 typical empty-state 40×40 nm^2 STM images for a 30-nm-thick anatase $TiO_{2-x}N_x$(001)-(1×4) film surface with [Figs. 4(b) and 4(e)] and without [Figs. 4(a) and 4(d)] a saturation dose of TMA and after visible-light irradiation for $x=0$ [Fig. 4(c)] and $x=0.02$ [Fig. 4(f)]. Undercoordinated Ti atoms along [010]-oriented ridges are visible as faint spots in the more magnified panel a′. The terraces prior to [Figs. 4(a) and 4(d)] dosing exhibit a few brighter spots which may be trace quantities of SrO. XPS reveals small amounts of SrO ($\leq\sim1\%$). The Sr presumably diffused out from the substrate where it may have been present in excess during growth. The presence of ~1% of SrO on the anatase (001) surface is unlikely to affect the photochemistry because SrO is a wide-gap material (5.9 eV) and the Hg emission lines are all below 5 eV photon energy. Moreover, quantum size effects associated with the small size of the SrO clusters on the anatase surface result in band gaps that exceed the bulk value. Individual TMA species bound to Ti sites along ridges are seen as brighter spots in the more magnified image b′ taken at the same area as a′, as well as in b and e. The majority of TMAs are spaced by 0.76 nm along [010], which is close to $2a_{ana}$. However, gaps are also seen as a result of missing TMAs along ridges. The mean TMA spacing along [100] is 1.5 nm which matches the spacing between ridges in the (1×4) reconstruction. As expected, visible light produces no significant diminution in surface TMA coverage for $x=0$ beyond the slight extent of thermally driven H-TMA recombination and desorption that occurs in the absence of light, as seen by comparing Figs. 4(b) and 4(c). In contrast, there is a marked reduction for $x=0.02$ [compare Figs. 4(e) and 4(f)], indicating visible-light photoactivity when the anatase is doped with N.

These results are placed on a quantitative footing by plotting TMA coverage (θ) vs light irradiation for $x=0$ and 0.02 in Fig. 5(a) for visible light, as well as combined visible and UV light. The differences are more clearly seen by plotting the logarithms of coverage vs light dose, as seen in Fig. 5(b). The slopes yield the rate constants for TMA photodecomposition. Comparing the data for the undoped and doped anatase surfaces shows that N doping only slightly reduces UV photoactivity. Thus, photogenerated holes in anatase are by and large *not* trapped at N sites, contrary to expectation if N 2*p*-derived states are strongly localized. The visible-light experiment corroborates this conclusion. When we irradiate with visible light that can only be absorbed at N sites where the local band gap is less than the photon energy, the doped specimen exhibits photoactivity, but the undoped specimen does not. Moreover, the TMA photodecomposition rate con-

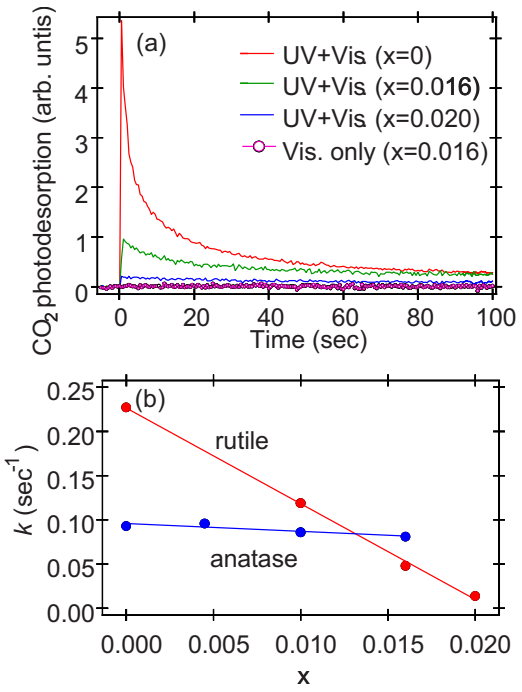

FIG. 6. (Color online) (a) Mass 44 photodecomposition spectra for TMA on epitaxial $TiO_{2-x}N_x$ rutile/TiO_2(110) for various x using UV-plus-visible light, along with visible light only for $x=0.016$; (b) initial mass 44 UV-plus-visible photodesorption rates for $TiO_{2-x}N_x$ anatase/$LaAlO_3$(001) and $TiO_{2-x}N_x$ rutile/TiO_2(110) as a function of x.

stants for N-doped anatase (001) are nearly the same for visible and visible plus UV light [Fig. 5(b)]. This result reveals that holes generated at N sites with visible light reach the surface at the same rate as those generated throughout the film with UV light. Thus, holes generated at N sites do not remain trapped there but rather readily diffuse to the surface.

In contrast, N doping of rutile (110) shuts down surface photoactivity altogether, as seen in Fig. 6(a). The initial UV-plus-visible CO_2 rate, corrected for TMA coverage by XPS (discussed below), falls off rapidly with increasing x. Moreover, visible light alone does not result in hole diffusion to the N-doped rutile (110) surface, as revealed by the absence of photoactivity at $x=0.016$ when visible light is used. A direct comparison of the UV-plus-visible initial photodecomposition rate constants (k) for anatase and rutile as a function of x [Fig. 6(b)] shows the stark difference in photoactivity between the two polymorphs. Here we fit the CO_2 photodesorption data to simple exponentials of the kind $r(t)=r_0\exp(-kt)$, where $r(t)$ and r_0 are the rates at time t and $t=0$ (initial light exposure time), respectively. In all cases, the data can be fitted to lines for the first 10 s of irradiation, with the slopes corresponding to k. The rate constant diminishes very slightly with x for anatase but falls to near zero for rutile at $x=0.02$, showing that UV-generated holes are impeded from reaching the surface to a much greater extent in rutile (110). Additionally, Fig. 6(b) shows that the photodecomposition rate constant for pure rutile (110) is larger than that of pure anatase (001) grown on $LaAlO_3$(001). Measurements for anatase grown on n-$SrTiO_3$(001) reveal rates comparable to those on rutile (110).[28] It is commonly thought

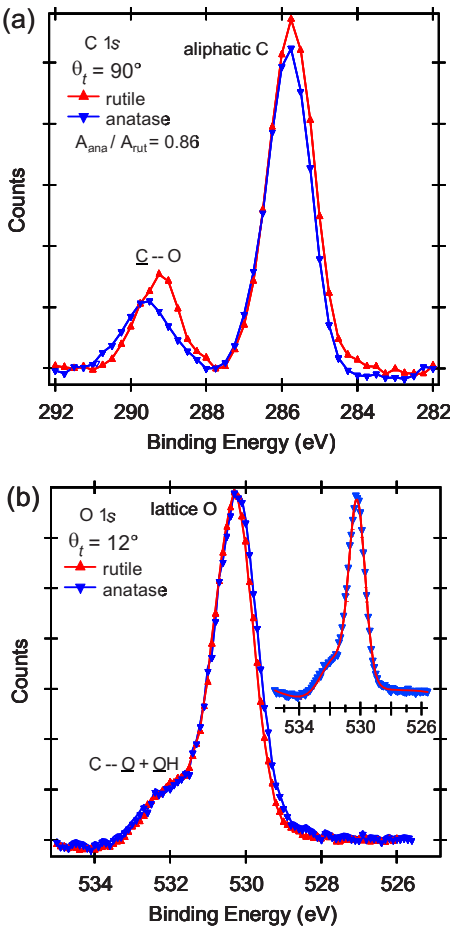

FIG. 7. (Color online) High-energy-resolution C 1s spectra at normal emission (a) ($\theta_t=90°$) and O 1s spectra at lower take-off angle (b) ($\theta_t=12°$) for saturation doses of TMA on epitaxial TiO_2 anatase/n-$SrTiO_3$(001) and TiO_2 rutile/TiO_2(110). Inset—curve fitting to separate the lattice and adlayer contributions to the O 1s spectrum for anatase (001).

that the photoactivity of anatase is greater than that of rutile. However, for the two crystal faces we have studied, undoped rutile is at least as active as undoped anatase. These results do not establish that rutile is as or more photoactive than anatase for *all* crystal faces, but they do help dispel the myth that anatase is *always* the more photoactive TiO_2 polymorph.

Accurate knowledge of the TMA coverage is essential for comparison of photoactivity for anatase and rutile as a function of N doping level, and we use C and O 1s core-level spectra (Fig. 7) to make this determination. We define 1.0 monolayer (ML) as the number density of surface Ti sites available to bind TMA, with 0.5 ML constituting saturation. The C 1s peak area for pure anatase (001) is ~86% of that for pure rutile (110) [Fig. 7(a)], revealing similar absolute coverages. This result is surprising because the STM images (Fig. 4) show TMA bound *only* to Ti sites on ridges of the anatase (001)−(1×4) surface. The Ti site density along these ridges is 1.75×10^{14} cm^{-2} which is three times lower than that on the unreconstructed rutile (110) surface (5.20×10^{14} cm^{-2}). This result establishes that TMA also sorbs in the troughs on anatase (001)−(1×4) and that these adsorbates are not visible to STM. There are two reasons why

TABLE I. Experimental and theoretical O 1*s* peak area ratios and resulting TMA coverages for pure rutile (110) and anatase (001) films.

	R_{exp}	R_{th}	TMA coverage[a]
Rutile (110)−(2×1)	0.21	0.32	0.33
Anatase (001)−(2×4)	0.20	0.23	0.43
Anatase (001)−(2×2)	0.20	0.33	0.30

[a]TMA coverage=$0.5(R_{exp}/R_{th})$.

TMA (or formate) in the troughs would not be visible to STM. First, if the TMA is less tightly bound in the troughs than along the ridges, it may be sufficiently mobile that it cannot be imaged by the relatively slowly moving STM tip. Indeed, the density-functional theory (DFT) calculations by Gong *et al.*[29] predict that the troughs are much less reactive toward carboxylates than the Ti ridges. Second, the corrugation of the surface may preclude TMA observation in the troughs. The corrugation along the 4× direction is sufficiently large that it is more difficult to image the troughs on the clean surface; Ti atoms along the ridges are much more easily imaged than those in the troughs. If TMA is sorbed to Ti atoms along the ridges as well as in the troughs, the corrugation is approximately the same as it is on the clean surface, and TMA in the troughs is not expected to be easily visible.

The same conclusion is reached by fitting the O 1*s* spectra [Fig. 7(b)]. We define the experimental O 1*s* peak area ratio R_{exp} as $A_{ad}/(A_{ad}+A_{lat})$ where A_{ad} and A_{lat} are the TMA/OH and lattice peak areas, respectively. We determine the TMA coverage by comparing R_{exp} with calculated values. In the simplest approach which ignores photoelectron diffraction effects, the theoretical O 1*s* peak area ratio (R_{th}) is

$$R_{th} = \frac{\sum_i N_i \exp(-d_i/\lambda \sin\theta_t)}{\sum_i N_i \exp(-d_i/\lambda \sin\theta_t) + \sum_j N_j \exp(-d_j/\lambda \sin\theta_t)}.$$

Here N_i and N_j are the numbers of oxygen per adlayer unit mesh associated with TMA plus OH (i) and the lattice (j), respectively, d_i and d_j are the layer depths, λ is the electron attenuation length, and the two sums run over discrete layers in the near-surface region. A saturation (2×1) TMA adlayer with the acid H bound to adjacent bridging oxygen was modeled for rutile (110).[30,31] For anatase (001), we modeled both (2×4) and (2×2) adlayers. In the (2×4) model, TMA binds only along Ti ridges on the (1×4) reconstructed surface, whereas TMA is also in troughs in the (2×2) model. Using λ=15 Å,[32] we arrive at the R_{th} values shown in Table I. The (2×2) adlayer model on anatase gives much better agreement with experiment in that the theoretical anatase: rutile TMA coverage ratio is 0.91, which compares reasonably well with the ratio of C 1*s* peak area ratio (0.86). In contrast, the (2×4) model gives a ratio of 1.30, which is considerably larger than the C 1*s* peak area ratio. Using the (2×2) results for anatase, we estimate that the absolute coverages $[0.5(R_{exp}/R_{th})]$ are ~0.3 ML for pure anatase and rutile. A TMA coverage less than 0.5 ML is consistent with a slow rate of TMAA desorption at 25 °C via recombination of TMA and surface-bound protons.[33,34] These results have implications for the TMA coverages determined by STM (Fig. 4). There are TMA molecules in the troughs of the anatase (001)−(1×4) surface detectable by XPS but invisible to STM. Therefore, the kinetics of TMA photodecomposition we observe by STM pertain only to those molecules that are bound to Ti sites along the ridges. However, the conclusions reached by STM were corroborated by an independent investigation using photodesorption spectroscopy which is sensitive to all TMA.

IV. SUMMARY

Using single-crystal epitaxial films of N-doped anatase (001) and rutile (110), we demonstrate a marked difference in visible-light photocatalytic activity between the two surfaces with respect to hole-mediated photodecomposition of trimethyl acetic acid. N doping activates the process in anatase (001) but not in rutile (110). For both polymorphs, N doping results in a redshift in the optical absorption spectrum which is presumably related to the generation of N 2*p* states that extend the valence band into the visible. The band gap is thus sufficiently low at least at N sites that visible-light photons can be absorbed there. The question then is whether or not such states are sufficiently localized that hole hopping to the surface is precluded, as qualitatively expected in light of the somewhat low N doping density (a maximum of ~1% of the oxygen is replaced by nitrogen in phase-pure films).

These experimental results clearly reveal that photogenerated holes created at N sites by visible light are not trapped there in anatase (001) but can hop to the surface and initiate photochemical reactions. However, this process does not occur in rutile (110). The outstanding question is why anatase is active and rutile is not.

This work on well-defined N-doped TiO_2 epitaxial films provides the first steps toward constructing structure/photochemical activity relationships for this class of materials. These results suggest that control over the process of hole diffusion to the surface might be gained by varying the surface orientation in either polymorph. That is, there may be orientations of rutile which show higher hole mobility than certain orientations of anatase. This possibility suggests that the choice of TiO_2 polymorph may be a secondary consideration to the crystallographic direction of hole hopping. Further experiments of this kind using other crystal faces of both polymorphs may allow the photoactivity of more structurally heterogeneous TiO_2 nanoparticle assemblies to be understood in a reductionist fashion.

Note added. The long-range periodicity of the TMA adlayer was not checked by low-energy electron diffraction in order to avoid beam-induced damage. The reconstruction designation given in the first column of Table I is what was modeled in the calculation of R_{th}.

ACKNOWLEDGMENTS

This work was performed in the Environmental Molecular Sciences Laboratory, a national scientific user facility sponsored by the Department of Energy's Office of Biological and Environmental Research and located at Pacific Northwest National Laboratory. This work was supported by the U.S. Department of Energy, Office of Science, Division of Chemical Sciences.

[1] A. Fujishima and K. Honda, Nature (London) **238**, 37 (1972).
[2] B. O'Regan and M. Gratzel, Nature (London) **353**, 737 (1991).
[3] M. Gratzel, Nature (London) **414**, 338 (2001).
[4] M. R. Hoffmann, S. T. Martin, W. Choi, and D. W. Bahnemann, Chem. Rev. (Washington, D.C.) **95**, 69 (1995).
[5] O. Carp, C. L. Huisman, and A. Reller, Prog. Solid State Chem. **32**, 33 (2004).
[6] R. Asahi, T. Morikawa, T. Ohwaki, K. Aoki, and Y. Taga, Science **293**, 269 (2001).
[7] C. Di Valentin, G. Pacchioni, and A. Selloni, Phys. Rev. B **70**, 085116 (2004).
[8] C. Di Valentin, G. Pacchioni, A. Selloni, S. Livraghi, and E. Giamello, J. Phys. Chem. B **109**, 11414 (2005).
[9] R. Asahi and T. Morikawa, Chem. Phys. **339**, 57 (2007).
[10] C. Di Valentin, E. Finazzi, G. Pacchioni, A. Selloni, S. Livraghi, M. C. Paganini, and E. Giamello, Chem. Phys. **339**, 44 (2007).
[11] E. Finazzi, C. Di Valentin, A. Selloni, and G. Pacchioni, J. Phys. Chem. C **111**, 9275 (2007).
[12] S. A. Chambers, S. H. Cheung, V. Shutthanandan, S. Thevuthasan, M. K. Bowman, and A. G. Joly, Chem. Phys. **339**, 27 (2007).
[13] S. H. Cheung, P. Nachimuthu, A. G. Joly, M. H. Engelhard, M. K. Bowman, and S. A. Chambers, Surf. Sci. **601**, 1754 (2007).
[14] S. A. Chambers, Surf. Sci. Rep. **39**, 105 (2000).
[15] S. H. Cheung, P. Nachimuthu, M. H. Engelhard, C. M. Wang, and S. A. Chambers, Surf. Sci. **602**, 133 (2008).
[16] M. Kawasaki, K. Takahashi, T. Maeda, R. Tsuchiya, M. Shinohara, O. Ishiyama, T. Yonezawa, M. Yoshimoto, and H. Koinuma, Science **266**, 1540 (1994).
[17] R. P. Vasquez, Surf. Sci. Spectra **1**, 24 (1992).
[18] J. J. Yeh and I. Lindau, At. Data Nucl. Data Tables **32**, 1 (1985).
[19] I. Lyubinetsky, Z. Q. Yu, and M. A. Henderson, J. Phys. Chem. C **111**, 4342 (2007).
[20] M. A. Henderson, J. M. White, H. Uetsuka, and H. Onishi, J. Am. Chem. Soc. **125**, 14974 (2003).
[21] R. D. Shannon, Acta Crystallogr. **32**, 751 (1976).
[22] S. Livraghi, A. Votta, M. C. Paganini, and E. Giamello, *Oxide Based Materials:, New Sources, Novel Phases, New Applications* (Elsevier, Amsterdam, 2005), Vol. 155, p. 375.
[23] S. Livraghi, A. Votta, M. C. Paganini, and E. Giamello, Chem. Commun. (Cambridge) **4**, 498 (2005).
[24] M. Batzill, E. H. Morales, and U. Diebold, Phys. Rev. Lett. **96**, 026103 (2006).
[25] S. Livraghi, M. C. Paganini, E. Giamello, A. Selloni, C. Di Valentin, and G. Pacchioni, J. Am. Chem. Soc. **128**, 15666 (2006).
[26] M. Batzill, E. H. Morales, and U. Diebold, Chem. Phys. **339**, 36 (2007).
[27] R. T. Haasch, T. Y. Lee, D. Gall, J. E. Greene, and I. Petrov, Surf. Sci. Spectra **7**, 193 (2000).
[28] T. Ohsawa, I. Lyubinetsky, M. A. Henderson, and S. A. Chambers, J. Phys. Chem. C **112**, 20050 (2008).
[29] X. Q. Gong, A. Sellonie, and A. Vittadini, J. Phys. Chem. B **110**, 2804 (2006).
[30] S. Thevuthasan, G. S. Herman, Y. J. Kim, S. A. Chambers, C. H. F. Peden, Z. Wang, R. X. Ynzunza, E. D. Tober, J. Morais, and C. S. Fadley, Surf. Sci. **401**, 261 (1998).
[31] D. I. Sayago, M. Polcik, R. Lindsay, R. L. Toomes, J. T. Hoeft, M. Kittel, and D. P. Woodruff, J. Phys. Chem. B **108**, 14316 (2004).
[32] S. Tanuma, C. J. Powell, and D. R. Penn, Surf. Interface Anal. **11**, 577 (1988).
[33] J. M. White and M. A. Henderson, J. Phys. Chem. B **109**, 12417 (2005).
[34] M. A. Henderson, J. M. White, H. Uetsuka, and H. Onishi, J. Catal. **238**, 153 (2006).